Energy Conversion and Management 65 (2013) 438–447

Contents lists available at SciVerse ScienceDirect

Energy Conversion and Management

journal homepage: www.elsevier.com/locate/enconman

Heat transfer analysis of a finned-tube evaporator for engine exhaust heat recovery

H.G. Zhang *, E.H. Wang, B.Y. Fan

College of Environmental and Energy Engineering, Beijing University of Technology, Pingleyuan No. 100, 100124 Beijing, China

ARTICLE INFO

Article history:
Received 8 July 2012
Received in revised form 16 August 2012
Accepted 7 September 2012

Keywords:
Finned-tube evaporator
Organic Rankine cycle
Waste heat recovery
Diesel engine
Heat transfer

ABSTRACT

The organic Rankine cycle (ORC) can be used to recover waste heat from an internal combustion engine. In such a system, the evaporator design is critical. Determining the amount of heat that can be transferred in a designed evaporator is extremely important for a successful ORC system. In this paper, the performance of a finned-tube evaporator used to recover exhaust waste heat from a diesel engine is presented. First, the exhaust heat of the chosen diesel engine is evaluated based on the measured data. Subsequently, a mathematical model of the evaporator is created based on the detailed geometry and the specific ORC working conditions. Then, the heat transfer of the evaporator is estimated as the diesel engine runs through all of its operating regions defined by the engine speed and the engine load. The results show that the exhaust temperature at the evaporator outlet increases with engine speed and engine load. Although the convective heat transfer coefficient of the organic working fluid is significantly larger than that of the exhaust gas, the overall heat transfer coefficient is slightly greater than that of the exhaust gas. Furthermore, the heat transfer rate is the greatest in the preheated zone and least in the superheated zone. Consequently, the heat transfer area for the preheated zone is nearly half of the total area. In addition, the area of the superheated zone is slightly greater than that of the two-phase zone. It is concluded that the heat transfer area for a finned tube evaporator should be selected carefully based on the engine's most typical operating region.

1. Introduction

Only a small portion of combustion energy becomes output from the crankshaft of an internal combustion engine; most of the energy is wasted in the exhaust and coolant systems. To improve the thermal efficiency of an internal combustion engine, an organic Rankine cycle (ORC) can be used to recover the waste heat. Several studies analyzing the ORC performances have been conducted recently [1–7]. One important challenge is determining how to bottom an ORC to an internal combustion engine to maximize energy efficiency during all operating regions of the engine. Results have been reported on applications with a gasoline engine [8,9] and a diesel engine [10,11].

Engine waste energy is transferred to the organic working fluid by an evaporator in an ORC, where the organic working fluid changes from a liquid state to a gas state under a high pressure. Subsequently, the organic working fluid, which has a high enthalpy, is expanded in an expander, and output power is generated. Therefore, the evaporator is a key component of the ORC for an engine waste-heat recovery system. The heat transfer effectiveness of the evaporator will influence the entire system's performance. Generally, there are two evaporator types used for waste heat recovery: the plate type and the shell-and-tube type. For a high temperature and pressure application, the finned-tube heat exchanger is widely used [12].

In this study, the performance of a finned-tube evaporator designed to recover the exhaust waste heat from a diesel engine is evaluated theoretically. R245fa is selected as the working fluid of the ORC. A mathematical model of the evaporator is established according to the detailed dimensions of the designed evaporator and the specified ORC working conditions. Then, the heat transfer of the finned-tube evaporator is estimated as the matched diesel engine runs through all of its operating regions defined by the engine speed and the engine load.

2. System description

The schematic of an ORC for exhaust heat recovery of a diesel engine is shown in Fig. 1. The fresh air is boosted by the compressor. Then, the air enters the engine cylinders, which combusts with the injected fuel. After expanding in the cylinders, the high-temperature gas is exhausted to the turbine to be expanded further. Here, at the turbine outlet, the temperature of the exhaust gas is still high between 200 °C and 600 °C. This high-temperature waste

Abbreviations: b.s.f.c., brake specific fuel consumption; LMTD, log mean temperature difference; ORC, organic Rankine cycle.

* Corresponding author. Tel.: +86 10 6739 2469; fax: +86 10 6739 2774.
E-mail address: zhanghongguang@bjut.edu.cn (H.G. Zhang).

0196-8904/$ - see front matter © 2012 Elsevier Ltd. All rights reserved.
http://dx.doi.org/10.1016/j.enconman.2012.09.017

Nomenclature

A	heat transfer area (m^2)
c	specific heat (J/kg K)
D	outer diameter (m)
d	inner diameter (m)
E, S	correction factor
f	resistance coefficient
G	mass flux (kg/m^2 s)
H	convective heat transfer rate (W/m^2 K)
h	enthalpy (kJ/kg)
l	tube length (m)
M	molecular weight (kg/kmol)
m	mass flow rate (kg/s)
mf	mass fraction
P	pressure (Pa)
Q	heat transfer rate (kW)
s	fin space (m)
T	temperature (K)
U	overall heat transfer coefficient (W/m^2 K)
w	vapor quality
x, y	molar amount
Re	Reynolds number
Pr	Prandtl number
Nu	Nusselt number

Greek letters

α	correction factor
γ	tube thickness (m)
δ	fin height (m)
η	efficiency
λ	thermal conductivity (W/m K)
μ	viscosity (kg/m s)
ρ	density (kg/m^3)

Subscripts

0	reference state
1, 2, 3, 4, 5, 6	state points for the R245fa
a, x, y, b	state points for the exhaust gas
exh	exhaust gas
f	fluid
g	gas
i	inner
l	liquid
lm	log mean
m	mean value
nb	nucleate boiling
o	outer
ph	preheated
ref	R245fa
sh	superheated
tp	two-phase
w	wall

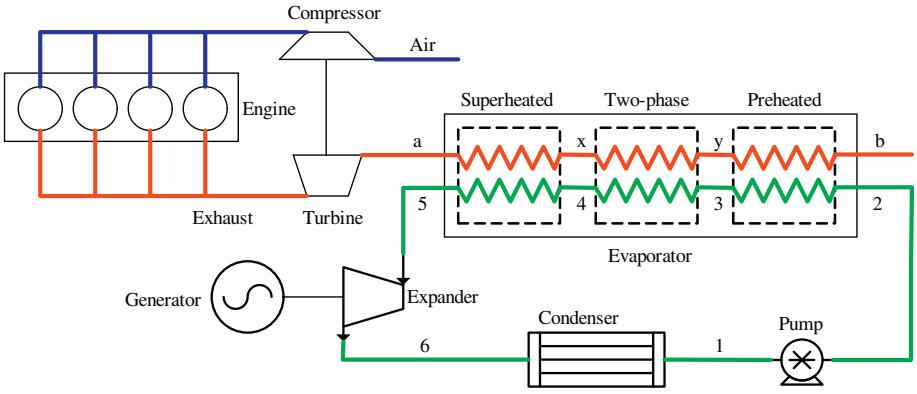

Fig. 1. Schematic of an ORC for engine exhaust heat recovery.

heat can be utilized via bottoming an ORC, where the evaporator is connected to the turbine outlet, which can be considered as a counter flow arrangement in this study. The actual layout is a cross flow arrangement. However, there are enough rows that it can be treated as a counter flow heat exchanger [13]. R245fa is used as the working fluid on the tube side of the evaporator because of its good safety and environmental properties [4]. The associated *T*–*s* diagram of the ORC is described in Fig. 2. Taking the practical operating conditions of a vehicle engine into account, the condensation temperature of the R245fa is set to 300 K in this investigation, and the evaporation pressure is set to 2.4 MPa. In the preheated zone, the sub-cooled liquid is heated to a saturated liquid state 3. Subsequently, the working fluid continues to evaporate to a saturated gas state 4 in the two-phase zone. Then, the saturated gas is heated further until the working fluid temperature increases to 25 °C. The ORC working parameters configured above

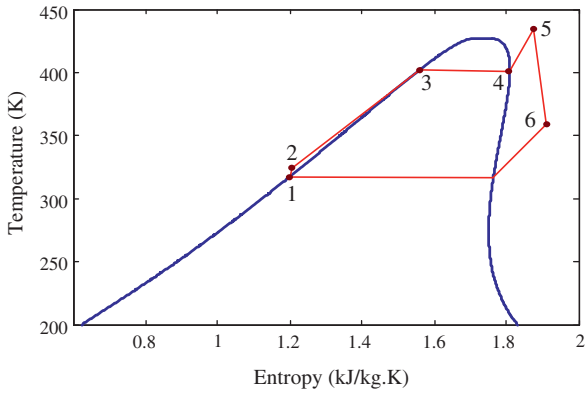

Fig. 2. *T*–*s* diagram of the ORC.

Table 1
Specification of the R425 diesel engine.

Item	Parameter	Unit
Model	R425	–
Displacement	2.499	L
Bore × stroke	92 × 94	mm
Cylinder number	4	–
Valve number per cylinder	4	–
Fuel injection equipment	Common rail injection system	–
Rated power	105	kW
Rated speed	4000	r/min
Max. torque	340	N m
Speed at max. torque	2000–2400	r/min

Table 2
Geometric dimensions of the finned-tube evaporator.

Item	Parameter	Unit
Number of tubes in row	5 or 6	–
Number of tube rows	9	–
Total number of tubes	50	–
Tube outside diameter	27	mm
Tube inner diameter	20	mm
Row pitch	46.77	mm
Tube pitch	54	mm
Fin density	50	m^{-1}
Fin height	27	mm
Fin thickness	4	mm
Total length with finned tubes	34	m
Tube material	Stainless steel	–
Fin material	Stainless steel	–
Tube row alignment	Staggered type	–
Internal heat transfer area	1.068	m^2
External unfinned area	1.154	m^2
Finned area	6.417	m^2
External total area	7.571	m^2

can be used to maximize the thermal efficiency of the ORC according to Ref. [14].

The designed evaporator is used on a turbocharged diesel engine, model type R425 manufactured by Jiangxi Jiangling Motor Group Co., Ltd. Table 1 gives the detailed specification of the R425 diesel engine. A finned-tube heat exchanger shown in Fig. 3 is designed to recover the engine exhaust heat. Table 2 lists the geometric dimensions of the finned-tube evaporator.

3. Mathematical model

To analyze the heat transfer of the finned-tube evaporator, when the R425 diesel engine is operating at various conditions, a mathematical model for the finned-tube evaporator is established. According to the ORC working parameters mentioned previously, the organic working fluid in the tube experiences three zones: the preheated zone, the two-phase zone, and the superheated zone. In the preheated zone, the R245fa is heated from the sub-cooled state 2 to the saturated liquid state 3. Accordingly, the exhaust gas is cooled from state *y* to state *b*. In the two-phase zone, the R245fa is heated from state 3 to the saturated gas state 4 while the exhaust gas is transferred from state *x* to state *y*. In the superheated zone, the R245fa continues to absorb the waste heat from the exhaust gas and changes from state 4 to a superheated gas state 5. Simultaneously, the exhaust gas varies from state *a* to state *x*.

The mathematical model gives a set of thermodynamic equations with regard to each zone of the evaporator. First, the thermodynamic properties of the exhaust gas and the R245fa are calculated for each zone based on the corresponding temperature and pressure. Second, the heat transfer rate for each zone is obtained according to energy equilibrium. Subsequently, considering the geometric dimensions of the evaporator, the convective heat transfer coefficients are estimated using the relative correlations. Then, the heat transfer area of each zone is determined. Moreover, when the engine's operating condition varies, the exhaust temperature and mass flow rate change accordingly. The variation of the heat transfer performance with the engine's operating condition is evaluated using the established evaporator model, which can provide a plausible reference to maximize the utilization of the exhaust waste heat.

3.1. Exhaust gas properties evaluation

The exhaust gas properties, which include the specific heat at constant pressure, the dynamic viscosity, and the thermal conductivity, must be determined for the heat transfer analysis. The main components in the exhaust gas of a diesel engine are CO_2, H_2O, N_2, and O_2. Moreover, the mass fractions of these components vary with the engine's operating condition. When the engine operates at steady state, the injected fuel quantity and the intake air amount can be measured on the engine test bench. Petroleum-derived diesel fuel is composed of approximately 75% saturated hydrocarbons and 25% aromatic hydrocarbons. Thus, the average chemical formula for common diesel fuel can be denoted by $C_{12}H_{23}$ [15]. Therefore, the combustion process of diesel fuel with air in the cylinders can be expressed simply as

$$xC_{12}H_{23} + y(O_2 + 3.76N_2) \rightarrow 12xCO_2 + 11.5xH_2O + 3.76yN_2 + (y - 17.75x)O_2 \quad (1)$$

The molar flow rates of the fuel and the intake air are calculated based on the measured mass flow rates. Consequently, the mole fractions for components CO_2, H_2O, N_2, and O_2 are obtained. The

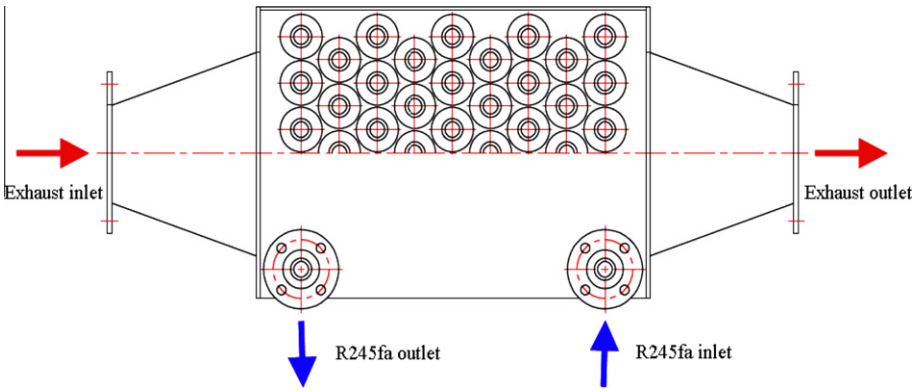

Fig. 3. Arrangement of the finned-tube evaporator.

corresponding mass fraction of each component can also be determined. If the exhaust temperature and pressure are measured, the specific enthalpy and the specific heat at constant pressure and the density for component i (i represents CO_2, H_2O, N_2, or O_2.) can be computed by REFPROP [16]. REFPROP, which was developed by the National Institute of Standards and Technology of the United States, is a program used to calculate the thermodynamic and transport properties of industrially important fluids and their mixtures with an emphasis on refrigerants and hydrocarbons. It implements three models for the thermodynamic properties of pure fluids: equations of state explicit in Helmholtz energy, the modified Benedict–Webb–Rubin equation of state, and an extended corresponding states (ECSs) model.

$$[h_i\ c_{p,i}\ \rho_i] = f(T_{exh}, P_{exh}, i) \tag{2}$$

Typically, the exhaust temperature is between 200 °C and 600 °C, and the exhaust pressure is slightly higher than atmospheric pressure. Therefore, the exhaust gas can be treated as a mixture of ideal gases [17]. Thus, the specific enthalpy and the specific heat of the exhaust gas can be calculated as

$$h_m = \sum_{i=1}^{4} mf_i h_i \tag{3}$$

$$c_{p,m} = \sum_{i=1}^{4} mf_i c_{p,i} \tag{4}$$

According to Amagat's law of additive volumes [17], the density of the exhaust gas is

$$\rho_m = \frac{\sum_{i=1}^{4} mf_i M_i}{\sum_{i=1}^{4} mf_i M_i/\rho_i} \tag{5}$$

Many heat transfer correlations require the Reynolds number and the Prandtl number. Therefore, the dynamic viscosity and the thermal conductivity of the exhaust gas should be estimated. If the exhaust temperature and pressure are known, the dynamic viscosity and the thermal conductivity for component i can be computed by REFPROP. Then, the Herning and Zipperer method can be used to calculate the exhaust viscosity [18]. The Wassiljewa equation is used to calculate the thermal conductivity of the exhaust gas [18].

3.2. Heat transfer rates calculation

Assuming that the exhaust temperature at state *b* is known, the exhaust enthalpy at state *b* can be calculated. Then, the overall heat transfer rate and the mass flow rate of the R245fa are determined by

$$Q = m_{exh}(h_a - h_b) = m_{ref}(h_5 - h_2) \tag{6}$$

The thermodynamic properties of the exhaust gas at state *x* and state *y* can also be calculated according to the energy equation for each zone. Hence, the heat transfer rates of all zones are obtained.

$$Q_{ph} = m_{exh}(h_y - h_b) = m_{ref}(h_3 - h_2) \tag{7}$$

$$Q_{tp} = m_{exh}(h_x - h_y) = m_{ref}(h_4 - h_3) \tag{8}$$

$$Q_{sh} = m_{exh}(h_a - h_x) = m_{ref}(h_5 - h_4) \tag{9}$$

3.3. Convective heat transfer coefficients

Considering the exhaust gas outside of the tubes, the convective heat transfer coefficient can be calculated with the Dias and Young correlation [19].

$$\frac{DH_{exh}}{\lambda_{exh}} = 0.1378\left(\frac{DG_{\max}}{\mu_{exh}}\right)^{0.718} \mathrm{Pr}_{exh}^{1/3}\left(\frac{S}{\delta}\right)^{0.296} \tag{10}$$

For the single-phase working fluid flowing in the tube, the Gnielinski correlation is used [20].

$$\mathrm{Nu}_f = \frac{\frac{f}{8}(\mathrm{Re}-1000)\mathrm{Pr}_f}{1+12.7\sqrt{\frac{f}{8}}(\mathrm{Pr}_f^{\frac{2}{3}}-1)}\left[1+\left(\frac{d}{l}\right)^{\frac{2}{3}}\right]\alpha \tag{11}$$

Considering the working fluid in the two-phase zone on the tube side, the experimental results show that the Liu and Winterton correlation accurately predicts the convective heat transfer coefficient of the R245fa [21]. Therefore, the Liu and Winterton correlation is used for the convective heat transfer coefficient in the two-phase zone.

$$H_{tp} = \sqrt{(EH_{f0})^2 + (SH_{nb})^2} \tag{12}$$

The correction factor for the film boiling is

$$E = \left[1 + w\mathrm{Pr}_l\left(\frac{\rho_l}{\rho_g} - 1\right)\right]^{0.35} \tag{13}$$

The convective heat transfer coefficient for film boiling H_{f0} is computed based on the Dittus-Boelter correlation [22].

The correction factor for the nucleate boiling is

$$S = \frac{1}{1 + 0.055E^{0.1}\mathrm{Re}_{f0}^{0.16}} \tag{14}$$

The Reynolds number corresponding to the saturated liquid state is expressed by

$$\mathrm{Re}_{f0} = \frac{G(1-w)d}{\mu_l} \tag{15}$$

The convective heat transfer coefficient for the nucleate boiling H_{nb} is calculated according to the pool boiling correlation of Copper [22].

3.4. Heat transfer areas

The overall heat transfer coefficient based on the tube outer surface is calculated as follows.

$$U = \frac{1}{\frac{A_o}{h_i A_i} + \frac{\gamma}{\lambda_w}\frac{A_o}{A_m} + \frac{1}{h_o \eta}} \tag{16}$$

The log mean temperature difference (LMTD) method is often used to predict the performance of a heat exchanger [23,24]. The LMTD is defined as

$$\Delta T_{lm} = \frac{\Delta T_1 - \Delta T_2}{\ln(\Delta T_1/\Delta T_2)} \tag{17}$$

where T_1 is the maximum temperature between two fluids at each end of the heat exchanger, and T_2 is the minimum temperature between the two fluids. Then, the heat transfer area is

$$A = \frac{Q}{U\Delta T_{lm}} \tag{18}$$

4. Results analysis

A program was created to evaluate the evaporator performance in Matlab according to the established mathematical model. The thermodynamic properties of the exhaust gas and the R245fa are calculated using REFPROP. The computation procedure is shown in Fig. 4. First, the mass flow rate and the thermodynamic properties of the exhaust gas at state *x* are calculated. Second, the

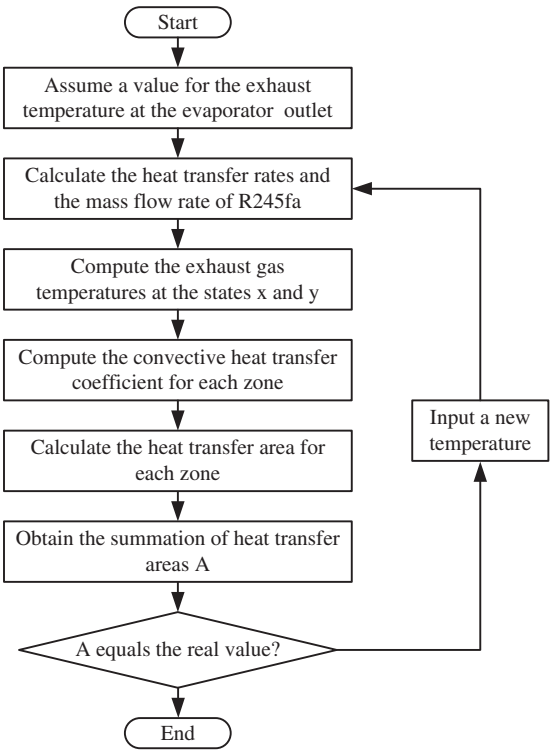

Fig. 4. Computation procedure for the mathematical model.

thermodynamic properties of the R245fa at state 2 and state 5 are determined based on the specific ORC working parameters. Third, an exhaust temperature value at state *y* is inputted. Accordingly, the overall heat transfer rate and the mass flow rate of the R245fa are computed according to energy equation. Then, the heat transfer rates for all three zones are calculated. Subsequently, the convective heat transfer coefficients of each zone are calculated according to the heat transfer correlations and the thermodynamic properties of the exhaust gas and the R245fa on each side. Furthermore, the overall heat transfer coefficient of each zone is obtained. Then, the heat transfer area for each zone is calculated using the LMTD method. If the summation of the three areas does not equal the actual area, a new exhaust temperature for state *b* is assumed again and a new iterative calculation is performed until the error of these two area values is less than 1%.

To evaluate the evaporator performance, we first obtain the waste heat quantities of the exhaust of the diesel engine. When a vehicle is running, the engine speed and load can vary through a wide range. Therefore, the engine performance test is conducted in an engine test cell to obtain the thermodynamic parameters for the exhaust, the intake air, and the coolant system over all engine operating regions, as defined by the engine speed and output torque. The test procedure is performed according to Ref. [25]. For the measurements described here, the minimum and maximum engine speeds are set to 1000 r/min and 4000 r/min, respectively. The intermediate speeds are selected using a step increment of 200 r/min. At each selected engine speed, eight different load values are selected, ranging from a 100% load to a minimum stable load value. The output power is measured using an eddy current

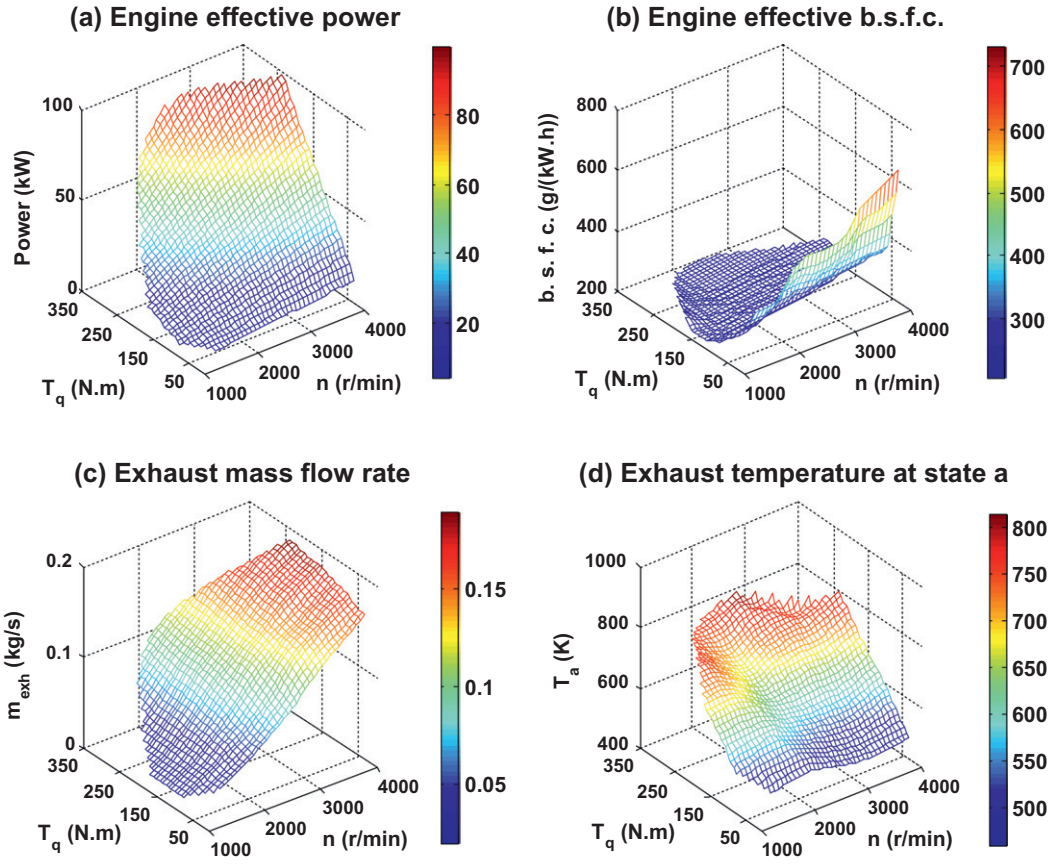

Fig. 5. Performance of the R425 diesel engine.

dynamometer manufactured by Xiangyi Power Testing Instrument Co., Ltd. (Model type GW300). The fuel consumption meter is also produced by Xiangyi Power Testing Instrument Co., Ltd. (Model type FC2212L). The exhaust temperature sensor is a *K* type thermocouple manufactured by Beijing Collihigh Technology Center Company. The mass flow rate of the intake air is measured using a thermal air-mass flow meter provided by Shanghai ToCeil Engine Testing Equipment Company (Model type ToCeil20N080). The high-speed data acquisition system is provided by Agilent Technologies Co., Ltd.

The measured engine data as a function of engine speed and engine load is shown in Fig. 5. Fig. 5a displays the engine power at the end of the flywheel. It can be seen that the output power increases with both engine speed and engine load, reaching 99.6 kW at the rated power point. The measured brake specific fuel consumption (b.s.f.c.) is shown in Fig. 5b. Apart from the operating region where the engine load is small and the engine speed is moderate or high, all the b.s.f.c. values are less than 240 g/kW h. The results indicate that the R425 diesel engine exhibits an excellent power performance and good fuel economy. The exhaust mass flow rate, which is the summation of the intake air mass flow rate and the fuel consumption rate, is shown in Fig. 5c. It can be seen that the exhaust mass flow rate increases slowly with engine load but rapidly with engine speed, which is because the increment of the engine load is primarily dependent on the improvement of the injected fuel quantity, whereas the mass flow rate of the intake air remains essentially constant for a stable engine speed. Fig. 5d shows the exhaust temperature at the evaporator inlet. The exhaust temperature increases slowly with engine speed but rapidly with engine load because the combustion energy improves significantly due to the large quantity of injected fuel for a high engine load. At the rated power point, the exhaust temperature is 528 °C.

The designed evaporator needs to operate under a high temperature and pressure condition with a small weight and a compact size. The most important condition is that it must recover enough waste heat from the engine exhaust gas so that the exhaust temperature can be reduced to near 100 °C. When combustion flue gas is cooled in a heat recovery application, the temperature must not be allowed to drop below the acid dew point. For this reason, it is better for the cooled exhaust temperature to be set above 100 °C. After the waste heat of the exhaust gas is obtained, the exhaust temperature at state *b* can be determined using the previous iterative calculation procedure. Accordingly, the specific enthalpies for state *a* and state *b* can be calculated. Furthermore, if the heat loss in the evaporator is neglected, the overall heat transfer rate in the evaporator is computed; the results are shown in Fig. 6a. The overall heat transfer rate increases with engine speed and engine load. This variation characteristic is similar to that of the engine power because the waste heat energy provided by the exhaust gas increases with engine power. At the rated power point, the overall heat transfer rate reaches 70.4 kW.

Simultaneously, the enthalpies of the R245fa at state 2 and state 5 are computed. Then, the mass flow rate of the R245fa is determined using Eq. (6), shown in Fig. 7a. The mass flow rate of the R245fa increases with engine speed and engine load. The variation tendency is similar to that of the overall heat transfer rate because the mass flow rate of the R245fa is proportional to the overall heat transfer rate when the previous ORC working parameters are fixed. At the rated power point, the mass flow rate of the R245fa reaches 0.221 kg/s.

Subsequently, the heat transfer rates for the preheated zone, the two-phase zone, and the superheated zone are calculated according to Eqs. (7)–(9). The results are shown in Fig. 6b, Fig. 6c, and Fig. 6d, respectively. The variation of the heat transfer rate for each

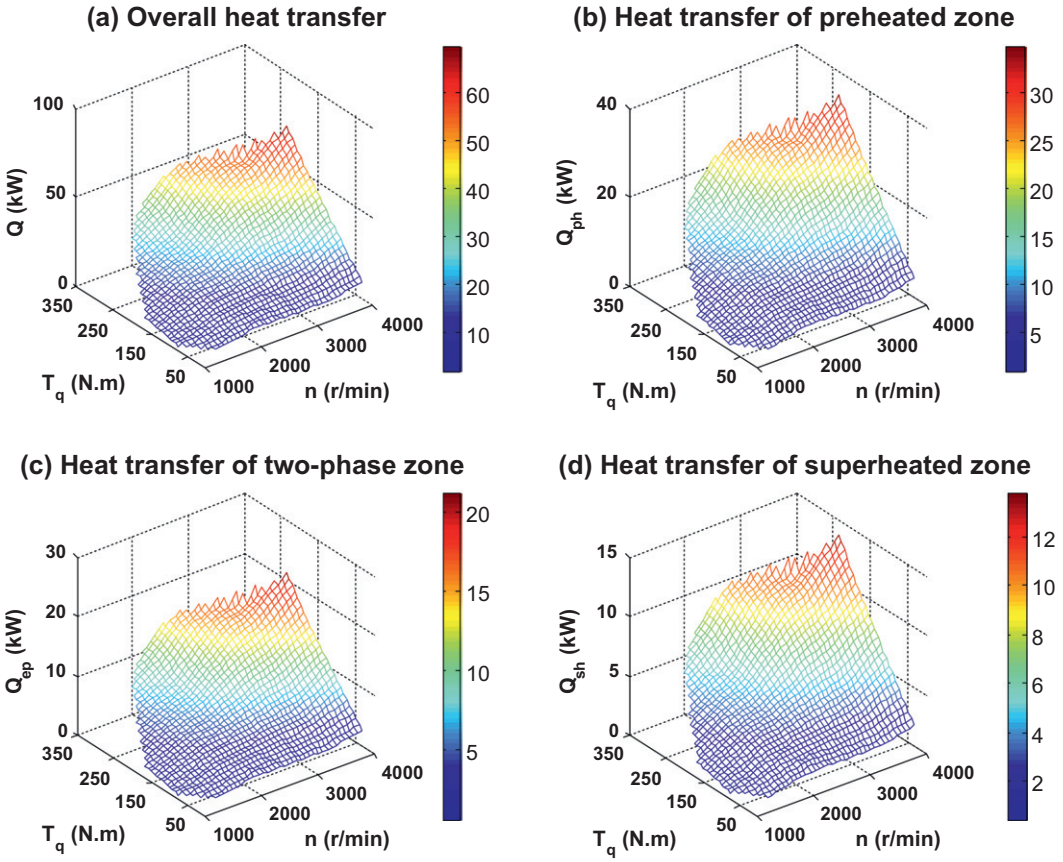

Fig. 6. Heat transfer rates of the evaporator.

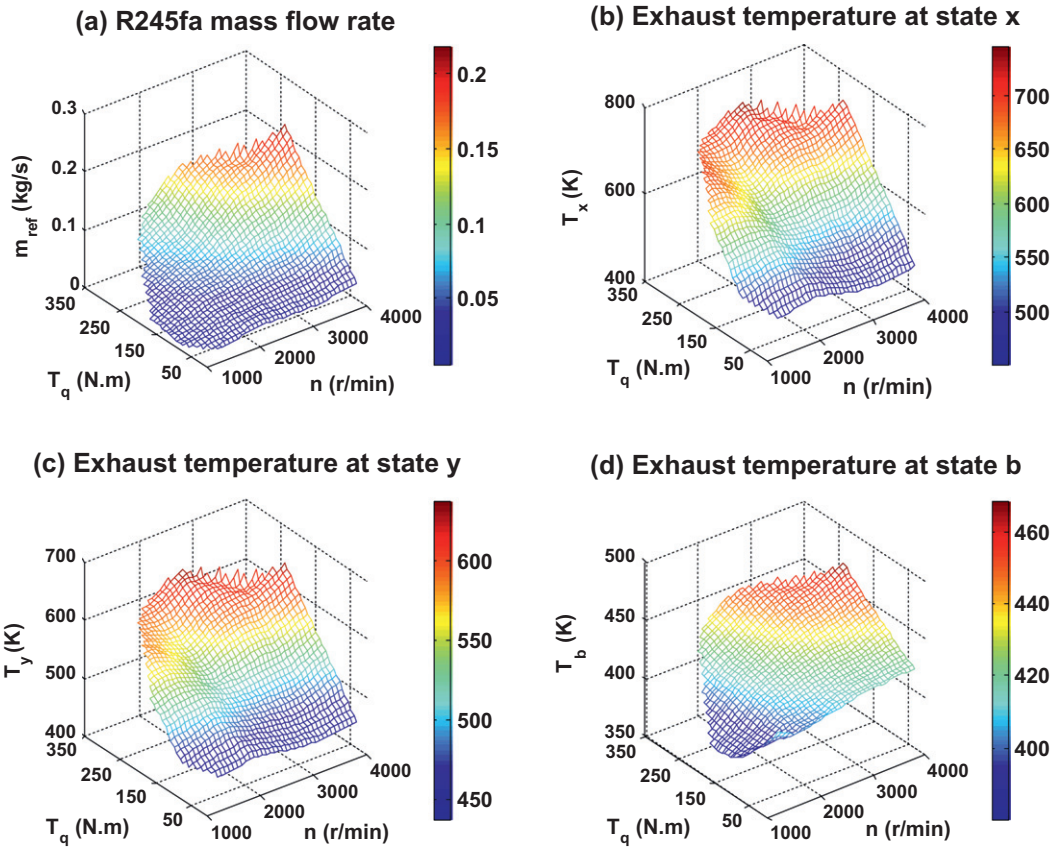

Fig. 7. Exhaust temperatures in the evaporator.

zone is consistent with that of the overall heat transfer rate across the entire engine's operating region because the heat transfer rate of each zone is also proportional to the mass flow rate of the R245fa. Furthermore, when the engine is working at steady state, the heat transfer rate of the preheated zone is the largest and that for the superheated zone is the smallest. The heat transfer rate of the preheated zone is close to the sum of the two-phase zone and the superheated zone. At the rated power point, the heat transfer rates of the preheated zone, the two-phase zone, and the superheated zone are 35.1 kW, 21.4 kW, and 13.9 kW, respectively.

Then, the enthalpy of the exhaust gas at each state can be determined using Eqs. (7)–(9). Afterwards, the related exhaust temperature is calculated according to the previous exhaust properties evaluation method. The exhaust temperatures at state *x*, state *y*, and state *b* are given in Fig. 7b, Fig. 7c, and Fig. 7d, respectively. The variations of the exhaust temperatures at state *x* and state *y* are similar to that of state *a* when the engine operating condition changes. However, the variation of the exhaust temperature at state *b* is close to that of the engine power because the magnitude of the heat transfer rate becomes larger and larger as the exhaust gas flows sequentially across the superheated zone, the two-phase zone, and the superheated zone. Thus, the exhaust temperature decreases more and more rapidly. At the rated power point, the exhaust temperatures at state *x*, state *y*, and state *b* are 465 °C, 365 °C, and 197 °C, respectively.

The exhaust temperature can be lowered to near 100 °C at the low engine speed and engine load region using the designed finned-tube evaporator. For example, the exhaust temperature decreases from 366 °C to 108 °C when the engine speed is 1000 r/min and the engine load is 127 Nm. However, the exhaust temperature at the evaporator outlet increases with engine power. At the rated power point, the exhaust temperature can only be reduced from 528 °C to 197 °C, which means that there is still waste energy that can be recovered because the engine is operating in the high power region. To evaluate the heat transfer efficiency of the finned-tube evaporator, the waste-heat recovery efficiency is introduced. Assuming the exhaust enthalpy is h_0, where the corresponding ex-

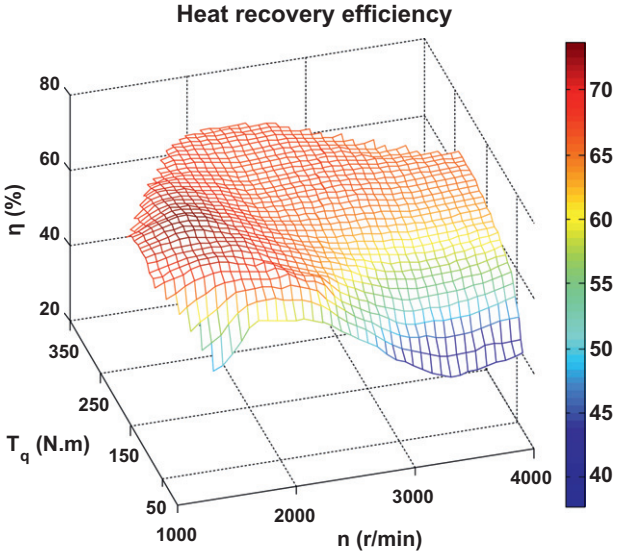

Fig. 8. Exhaust heat recovery efficiency.

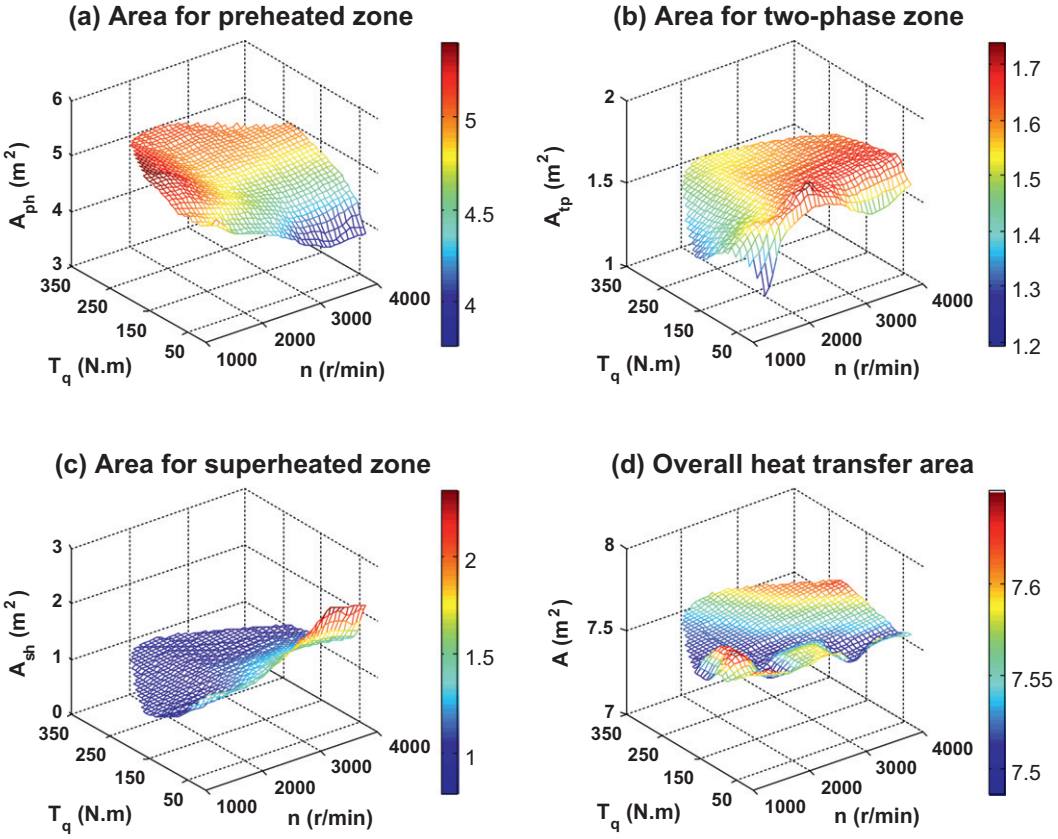

Fig. 9. Estimated heat transfer surface areas.

haust temperature is 101 °C, the waste-heat recovery efficiency is defined as

$$\eta = \frac{Q}{m_{exh}(h_a - h_0)} \tag{19}$$

where Q is the overall heat transfer rate. The calculated waste-heat recovery efficiency of the evaporator is shown in Fig. 8. The waste-heat recovery efficiency decreases slightly as the engine speed increases. The waste-heat recovery efficiency is between 60% and 70% for most of the engine's operating region. At the rated power point, this efficiency equals 64.1%. When the engine operates at a high engine speed and small engine load region, the waste-heat recovery efficiency drops because the overall heat transfer coefficient in the preheated zone decreases and the exhaust temperature at the evaporator outlet rises.

Despite the waste-heat recovery efficiency essentially not changing with the engine power, much of that waste heat energy can still be recovered in the high engine power region because the exhaust-waste heat energy increases significantly in the high engine power region. To improve the recovery energy further, the heat transfer area of the evaporator should be increased, which will cause the exhaust temperature at state *b* to be less than 100 °C in the small engine power region. Therefore, when the working conditions of the ORC are specified, the heat transfer area of the evaporator should be designed carefully based on the engine's operating region that is most likely to occur.

The heat transfer areas of the preheated zone, the two-phase zone, and the superheated zone can be calculated using Eqs. (17) and (18). The results are shown in Fig. 9. At the rated power point, the heat transfer areas of the preheated zone, the two-phase zone, and the superheated zone are 4.99 m^2, 1.60 m^2, and 1.02 m^2, respectively. The heat transfer area of the preheated zone is the largest, which is almost half of the total area. The heat transfer area of the two-phase zone is slightly greater than that of the superheated zone primarily caused by the discrepancies of the heat transfer rates. In addition, Fig. 9d shows the calculated total heat transfer area. The maximum relative error to the real area is 0.9%, which verifies the iterative calculation procedure is plausible.

The locations where the R245fa is in the saturated liquid state and the saturated gas state in the tubes vary with the engine operating point. In the low-speed region, the heat transfer area of the preheated zone increases, whereas it reduces in the two-phase zone. The reason can be explained as below. Both the overall heat transfer coefficient and the average temperature difference for the two-phase zone increase in the low-speed region, which decreases the heat transfer area according to Eq. (18). On the contrary, the overall heat transfer coefficient and the average temperature difference of the preheated zone decrease. Considering the superheated zone, the overall heat transfer coefficient decreases while the average temperature difference increases, which results in the heat transfer area of the superheated zone changing very little in the low-speed region. Additionally, the results show that the heat transfer areas of the preheated zone and the two-phase zone decrease while that for the superheated zone increases when the engine speed is large and the engine load is small. The reason can be explained as below. In the preheated zone, the average temperature difference increases and the overall heat transfer coefficient changes little, which cause the heat transfer area to decrease. For the two-phase zone, the overall heat transfer coefficient increases and the average temperature difference decreases. The calculated heat transfer area reduces slightly according to

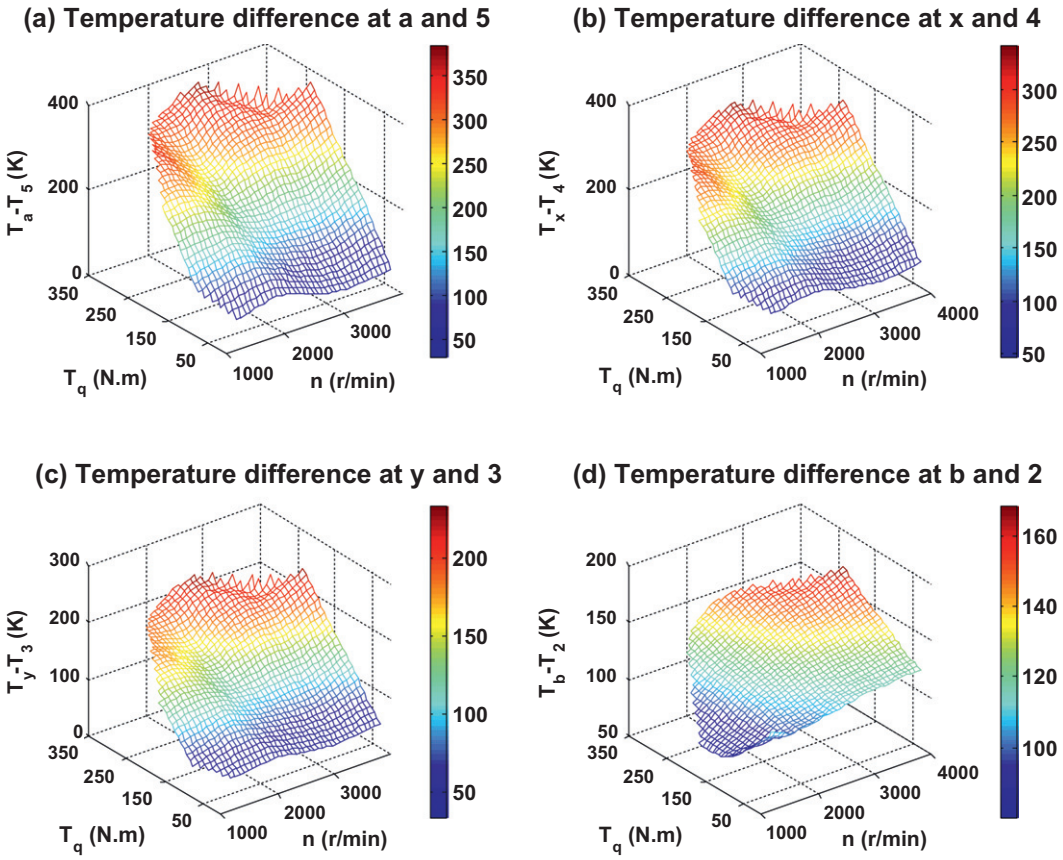

Fig. 10. Temperature differences between the exhaust gas and the R245fa.

Eq. (18). In the superheated zone, both the overall heat transfer coefficient and the average temperature difference decrease. Thus, the heat transfer area increases significantly.

The temperature difference between the exhaust gas and the R245fa at any position in the evaporator tubes should be greater than a certain value due to the pinch point analysis [26,27]. The results of the temperature differences at state *a*, state *x*, state *y*, and state *b* are given in Fig. 10. The variation of the temperature difference at each state is consistent with that of the corresponding exhaust temperature because the relative working temperature of the R245fa remains constant as the engine operating condition varies. When the engine operates in steady state, the mass fraction of each component in the exhaust gas does not alter. Therefore, the temperature variation of the exhaust gas is proportional to the corresponding heat transfer rate. Considering the heat transfer process between the exhaust gas and the R245fa, the pinch point can only occur at state *a*, state *x*, state *y*, or state *b*. The results indicate that the pinch point may occur at any of these four states because the mass fraction of each component varies with the engine operating condition, which results in the variation of the exhaust specific heat. In addition, the results show that all the temperature differences are greater than 30 °C, which satisfy the requirement for the pinch point temperatures.

5. Conclusions

In this study, the heat transfer characteristics of an ORC evaporator applied on an R425 diesel engine were analyzed using measured data. A mathematical model was setup with regard to the preheated zone, the two-phase zone, and the superheated zone of a finned-tube evaporator. The performance of the evaporator was evaluated over the engine's entire operating region. Based on our analysis, the followings can be concluded:

1. The overall heat transfer rate of the evaporator increases with engine power and reaches 70.4 kW at the rated power point. The mass flow rate of the R245fa increases linearly with the overall heat transfer rate, which reaches 0.221 kg/s at the rated power point. The heat transfer rate of the preheated zone is the largest and is nearly half of the overall heat transfer rate. The heat transfer rate of the two-phase zone is slightly higher than that of the superheated zone. Furthermore, the heat transfer rate of each zone is proportional to that of the overall heat transfer rate when the engine operating condition changes.
2. In the evaporator, the exhaust temperature decreases gradually as the exhaust gas flows sequentially across the superheated zone, the two-phase zone, and the preheated zone. The exhaust temperature can be reduced to near 100 °C when the engine operates in the low engine speed and engine load region. Furthermore, the exhaust temperature at the evaporator outlet increases with the engine power. At the rated power point, the exhaust temperature can only be reduced to 197 °C. Moreover, the waste-heat recovery efficiency decreases slightly from 70% to 60% as the engine speed increases. Therefore, the residual waste-heat energy in the exhaust gas increases with engine power.
3. The heat transfer area of the preheated zone is the largest, which is almost half of the total area. The heat transfer area of the two-phase zone is slightly higher than that of the superheated zone. Moreover, the locations where the R245fa is in the saturated liquid state and the saturated gas state in the tubes vary with engine operating condition. In the low-speed region, the heat transfer area of the preheated zone increases, whereas

that for the two-phase zone decreases. Additionally, the heat transfer areas of the preheated zone and the two-phase zone decrease, whereas that of the superheated zone increases when the engine speed is large and the engine load is small.

4. All the temperature differences are greater than 30 °C, which fulfills the requirement for the pinch point temperatures. Moreover, the pinch point may occur at any of the states included *a*, *x*, *y*, and *b*.

Acknowledgements

This work was sponsored by the National Basic Research (973) Program of China (Grant Nos. #2011CB707202 and #2011CB710704), the National High-Tech Research and Development Program of China (863 Program) (Grant No. 2009AA05Z206), and the Funding Project for Academic Human Resources Development in Institutions of Higher Learning Under the Jurisdiction of Beijing Municipality (Grant No. PHR201008019).

References

[1] Kang SH. Design and experimental study of ORC (organic Rankine cycle) and radial turbine using R245fa working fluid. Energy 2012;41(1):514–24.
[2] He C, Liu C, Gao H, Xie H, Li Y, Wu S, et al. The optimal evaporation temperature and working fluids for subcritical organic Rankine cycle. Energy 2012;38:136–43.
[3] Sun J, Li W. Operation optimization of an organic Rankine cycle (ORC) heat recovery power plant. Appl Therm Eng 2011;31:2032–41.
[4] Wang EH, Zhang HG, Fan BY, Ouyang MG, Zhao Y, Mu QH. Study of working fluid selection of organic Rankine cycle (ORC) for engine waste heat recovery. Energy 2011;36(5):3406–18.
[5] Rentizelas A, Karellas S, Kakaras E, Tatsiopoulos I. Comparative techno-economic analysis of ORC and gasification for bioenergy applications. Energy Convers Manage 2009;50:674–81.
[6] Gewald D, Karellas S, Schuster A, Spliethoff H. Integrated system approach for increase of engine combined cycle efficiency. Energy Convers Manage 2012;60:36–44.
[7] Vélez F, Chejne F, Antolin G, Quijano A. Theoretical analysis of a transcritical power cycle for power generation from waste energy at low temperature heat source. Energy Convers Manage 2012;60:188–95.
[8] Wang T, Zhang Y, Jie Z, Shu G, Peng Z. Analysis of recoverable exhaust energy from a light-duty gasoline engine. Appl Therm Eng 2012. http://dx.doi.org/10.1016/j.applthermaleng.2012.03.025.
[9] Wang EH, Zhang HG, Zhao Y, Fan BY, Wu YT, Mu QH. Performance analysis of a novel system combining a dual loop organic Rankine cycle (ORC) with a gasoline engine. Energy 2012;43:385–95.
[10] Katsanos CO, Hountalas DT, Pariotis EG. Thermodynamic analysis of a Rankine cycle applied on a diesel truck engine using steam and organic medium. Energy Convers Manage 2012;60:68–76.
[11] Hountalas DT, Mavropoulos GC, Katsanos C, Knecht W. Improvement of bottoming cycle efficiency and heat rejection for HD truck applications by utilization of EGR and CAC heat. Energy Convers Manage 2012;53:19–32.
[12] Webb RL, Kim NH. Principles of enhanced heat transfer. 2nd ed. New York: Taylor & Francis; 2005.
[13] Shi MZ, Wang ZZ. Principle and design of heat exchangers. 4th ed. Nanjing: Southeast University Press; 2009 [in Chinese].
[14] Wang E, Zhang H, Fan B, Wu Y. Optimized performances comparison of organic Rankine cycles for low grade waste heat recovery. Journal of Mechanical Science and Technology 2012;26:2301–12.
[15] Wikipedia, Diesel fuel. <http://en.wikipedia.org/wiki/Diesel_fuel>, 2012-04-20.
[16] REFPROP version 8.0, NIST standard reference database 23. The US Secretary of Commerce, America; 2007.
[17] Cengel YA, Boles MA. Thermodynamics an engineering approach. 6th ed. London: McGraw-Hill; 2008. p. 681–709.
[18] Poling BE, Prausnitz JM, O'Connell JP. The properties of gases and liquids. 5th ed. New York: McGraw-Hill; 2001.
[19] Gu WZ, Shen JR, Ma CF, Zhang YM. Enhanced heat transfer. Beijing: Science Press; 1990 [in Chinese].
[20] Gnielinski V. New equations for heat mass transfer in turbulent pipe and channel flows. Int Chem Eng 1976;16:359–68.
[21] Wang X, Wang H, Wang H. Experimental study on evaporating heat transfer characteristics of HFC-245fa. J Wuhan Univ Technol 2011;33(3):67–71.
[22] Ghiaasiaan SM. Two-phase flow, boiling and condensation in conventional and miniature systems. New York: Cambridge University Press; 2008.
[23] Bergman TL, Lavine AS, Incropera FP, Dewitt DP. Fundamentals of heat and mass transfer. 7th ed. USA: John Wiley & Sons; 2011.
[24] Ghazi M, Ahmadi P, Sotoodeh AF, Taherkhani A. Modeling and thermo-economic optimization of heat recovery heat exchangers using a multimodal genetic algorithm. Energy Convers Manage 2012;58:149–56.
[25] National standard of the People's Republic of China. GB/T 18297–2001; 2001.
[26] Kemp IC. Pinch analysis and process integration: a user guide on process integration for the efficient use of energy. 2nd ed. Beijing: Chemical Industrial Press; 2006.
[27] Wu W, Zhao L, Ho T. Experimental investigation on pinch points and maximum temperature differences in a horizontal tube-in-tube evaporator using zeotropic refrigerants. Energy Convers Manage 2012;56:22–31.